

Modulation of *in vivo* muscle power output during swimming in the African clawed frog (*Xenopus laevis*)

Christopher T. Richards* and Andrew A. Biewener

Harvard University, 100 Old Causeway Road, Bedford, MA 01730, USA

*Author for correspondence (e-mail: richards@fas.harvard.edu)

Accepted 3 July 2007

Summary

The goal of this study is to explore how swimming animals produce the wide range of performance that is seen across their natural behaviors. *In vivo* recordings of plantaris longus muscle length change were obtained by sonomicrometry. Simultaneous with muscle length data, force measurements were obtained using a novel tendon buckle force transducer placed on the Achilles tendon of *Xenopus laevis* frogs during brief accelerating bursts of swimming. *In vivo* work loops revealed that the plantaris generates a variable amount of positive muscle work over a range of swimming cycle durations (from 0.23 to 0.76 s), resulting in a large range of cycle power output (from 2.32 to 74.17 W kg⁻¹ muscle). Cycle duration correlated negatively with cycle power, and cycle work correlated positively (varying as a function of peak cycle stress and, to a much lesser extent, fascicle strain amplitude). However, variation in cycle duration only contributed to 12% of

variation in power, with cycle work accounting for the remaining 88%. Peak cycle stress and strain amplitude were also highly variable, yet peak stress was a much stronger predictor of cycle work than strain amplitude. Additionally, EMG intensity correlated positively with peak muscle stress ($r^2=0.53$). Although the timing of muscle recruitment (EMG phase and EMG duty cycle) varied considerably within and among frogs, neither parameter correlated strongly with cycle power, cycle work, peak cycle stress or strain amplitude. These results suggest that relatively few parameters (cycle duration, peak cycle stress and strain amplitude) vary to permit a wide range of muscle power output, which allows anurans to swim over a large range of velocities and accelerations.

Key words: muscle, force, sonomicrometry, work, power, plantaris, frog, *Xenopus laevis*.

Introduction

Animals that move over a wide range of speeds experience variable forces on their body, requiring them to modulate muscle work and power output. Running animals, for example, increase muscle work to move up inclines (Roberts et al., 1997), to increase speed (Daley and Biewener, 2003) and to accelerate (Roberts and Scales, 2004). Similarly, flying birds modulate work and power output to accommodate changes in aerodynamic power requirements over different flight speeds (Hedrick et al., 2003). Modulation of muscle work and power probably also enables aquatic animals to overcome varying hydrodynamic forces as they swim over a range of speeds. However, few studies have directly measured muscle power output *in vivo* during swimming, and none have done so within the context of acceleration and changes in swimming speed. Partly, this reflects the difficulty of making such measurements in swimming fish and other aquatic animals. This study therefore aims to explore how *in vivo* muscle force, length change and activation dynamics vary to modulate muscle power output during anuran swimming. To achieve this, we analyze the plantaris longus muscle of African clawed frogs (*Xenopus laevis*) during short accelerating bursts of swimming.

A number of recent studies have investigated how muscles

generate the mechanical power required for swimming. Research on axial muscle performance in carp (*Cyprinus carpio*) during steady swimming has suggested that the activation and length change patterns (estimated from kinematics), when duplicated under *in vitro* conditions, allow the muscles to shorten at a velocity that maximizes their power output (Rome et al., 1988). Direct measurements of muscle length changes by sonomicrometry have validated kinematic estimates based on spinal flexion (Coughlin et al., 1996a), but did not measure muscle force *in vivo*. Marsh et al. (Marsh et al., 1992) used *in vivo* measurements of hydrodynamic pressure within the mantle cavity of scallops (*Argopecten irradians* and *Chlamys hastata*) and sonomicrometry to provide some of the first direct measurements of power output by the adductor muscle during jet propulsion. Subsequently, Biewener and Corning (Biewener and Corning, 2001) gathered *in vivo* measurements of lateral gastrocnemius force and length dynamics in mallard ducks (*Anas platyrhynchos*) to determine how this muscle shifts its contractile performance to meet the differing demands for mechanical work and power output during terrestrial locomotion *versus* swimming. These studies on scallops and mallards are consistent with earlier *in vitro* work loop studies (Altringham and Johnston, 1990a; Luiker and

Stevens, 1991; Luiker and Stevens, 1993; Rome et al., 1993), showing that muscles shorten significantly during force production to generate the power required for swimming. Although these studies provide insight into how *in vivo* muscle force and length patterns interact to produce work and power, they do not address how muscles vary these patterns to produce the wide range of performance seen in natural swimming.

A general goal of our work is to explore the mechanisms by which the neuromuscular system modulates performance by observing how parameters such as muscle force, shortening velocity and motor recruitment relate to muscle power output. For animals that use muscle shortening–lengthening cycles to drive oscillatory swimming motions, cycle power is calculated from the average work produced during a cycle (net cycle work) divided by the cycle duration. Therefore, a muscle can increase power output from one cycle to the next by increasing cycle work (by increasing net muscle force and/or shortening) and/or decreasing cycle duration. To enable flight over a range of speeds, in flying cockatiels net power output of the pectoralis muscle was found to vary mainly through changes in work output per wing beat cycle and to a much lesser extent *via* changes in cycle duration (Hedrick et al., 2003). In contrast, several fish species increase swimming speed by decreasing the duration of the contraction cycles of their axial musculature, thereby increasing tail beat frequency (Brill and Dizon, 1979; Rome et al., 1984; Altringham and Ellerby, 1999; Swank and Rome, 2000). Because muscle power is highly dependent on cycle duration (Altringham and Johnston, 1990a; Coughlin et al., 1996b; Altringham and Block, 1997; Rome et al., 2000; Syme and Shadwick, 2002), we hypothesize that, in contrast to the modulation of power output during flight (Hedrick et al., 2003), cycle duration will be a key determinant of power output of the plantaris longus of swimming *X. laevis* frogs.

Anurans provide an ideal model for investigating, *in vivo*, how muscles generate the mechanical output necessary for overcoming the hydrodynamic demands of swimming. Although previous studies have addressed muscle function in swimming fish, these studies are limited because axial and myotomal muscle forces cannot be measured directly under *in vivo* conditions. Consequently, current knowledge of muscle power modulation during swimming is largely based on *in vitro* studies. In contrast, the plantaris longus muscle of anurans enables direct measurements of muscle power *in vivo*. Moreover, there is a rich history of work in muscle physiology using isolated anuran muscles (Hill, 1970), as well as a strong body of work addressing *in vivo* hindlimb muscle strain and activation patterns in swimming anurans (Kamel et al., 1996; Gillis and Biewener, 2000; Gillis, 2007). Additionally, many anurans have large hindlimb musculature, which facilitates electrode implantation. For this study, we chose *Xenopus laevis* because it is an obligatorily aquatic frog that uses bursts of ‘kick-and-glide’ swimming to prey on small fish and escape from birds and other predators (Lafferty and Page, 1997). *X. laevis*, like many anurans, has a prominent plantaris muscle that transmits propulsive force to the foot *via* a long Achilles tendon. Therefore, unlike the axial musculature of fish, *in vivo* muscle force measurements can be made directly by mounting a calibrated force transducer on the plantaris muscle’s tendon.

In this study, we report the use of a novel tendon force

transducer to make the first observations of time-varying patterns of muscle force simultaneous with muscle length and muscle activation during anuran swimming. We use these recordings to test the hypothesis that changes in muscle power occur not only *via* changes in muscle work (increased force and shortening strain), but also by increasing shortening velocity to reduce the stroke cycle duration. We also explore how the magnitude and timing of neural recruitment affects the dynamics of the muscle’s *in vivo* force–length behavior.

Materials and methods

Animals

Adult female *Xenopus laevis* Daudin 1802 frogs ($N=6$; 150.5 ± 31.0 g mean body mass \pm s.d., Table 1) were obtained from Xenopus Express, Inc. (Plant City, FL, USA). Animals were housed in aquaria at the Concord Field Station and maintained at 20–22°C under a 12 h:12 h light:dark cycle. During experiments, animals were allowed to swim freely in an 80 cm \times 96 cm Plexiglas™ tank filled to a relatively shallow water height of 5–6 cm to encourage horizontal swimming. To elicit a range of swimming speeds, animals were stimulated to swim either by gentle tapping of the feet (slow swimming trials) or by dropping a small plastic block behind the feet (fast swimming trials). Trials in which frogs either turned sharply or collided with the tank walls were not included in the analysis. All swimming trials were carried out at room temperature (20–22°C). Surgical and experimental protocols were approved by the Harvard University Institutional Animal Care and Use Committee.

Surgical procedures

Frogs were anesthetized for 10–15 min in tapwater containing 0.1% tricaine methane sulphonate (MS-222) at room temperature, pH 7.0. After being sedated, a small incision was made through the skin distal to the ankle on the medial surface of the right leg. After exposing the distal portion of the Achilles tendon, a small (~5 mm) incision was made through the connective tissue sheath on either side of the Achilles tendon. A small (2 \times 5 mm) custom force buckle transducer (Fig. 1A, see below) was implanted on the inner surface of the tendon with the bare surface of the buckle against the tendon. Two 4-0 silk suture ties were securely fastened around the tendon. To prevent chafing of the tendon, both sutures were threaded through a small piece of polyethylene tubing (1.22 mm outer diameter; Clay Adams, Parsippany, NJ, USA) cut to the width of the tendon (see Fig. 1A).

Table 1. *Plantaris* muscle morphological data

Frog	Body mass (g)	Muscle		
		Mass (g)	Cross-sectional area (cm ²)	Resting length (mm)
1	126	2.05	0.62	31.39
2	179	3.83	1.15	34.18
3	171	3.55	1.00	33.35
4	143	3.08	1.04	27.97
5	119	2.28	0.69	31.17
6	142	3.22	0.90	33.6
Mean \pm s.d.	147 \pm 24	3.00 \pm 0.70	0.90 \pm 0.21	31.94 \pm 2.30

Next, a ~2 cm incision was made through the skin covering the plantaris longus muscle. Using a pair of forceps, two small openings (spaced 7–9 mm apart) were made in the central region of the muscle along a single fascicle spanning the entire muscle length. A pair of 1.0 mm diameter sonomicrometry crystals (Sonometrics Corporation, Ontario, Canada) were positioned in the holes and tied into place using 6-0 silk suture threaded through the muscle epimysium. An additional suture threaded through the muscle surface further immobilized the crystal lead wires, preventing motion artifact from wire movement.

Silver electromyography (EMG) wires (California Fine Wire Company, Grover Beach, CA, USA) were formed into a hook (0.5 mm bared tips, spaced apart by 5 mm) and inserted into the

muscle using a 23-gauge hypodermic syringe needle. EMG wires were tied to the muscle epimysium using 6.0 silk suture.

After closing each surgical incision, lead wires for the force transducer, sonomicrometry crystals and EMG electrodes were anchored with 4-0 silk suture to the skin at intervals along the leg and trunk to provide stress relief.

Kinematics and high speed video

Frogs were filmed at 125 frames s^{-1} at a 1/250s shutter speed using a high-speed Photron Fastcam camera (Photron Ltd, San Diego, CA, USA). A 3×3 cm rectangular grid placed beneath the floor of the swimming tank provided calibration for the video images. For three of the six frogs, swimming kinematics data were obtained from a 1.0 mm diameter white marker

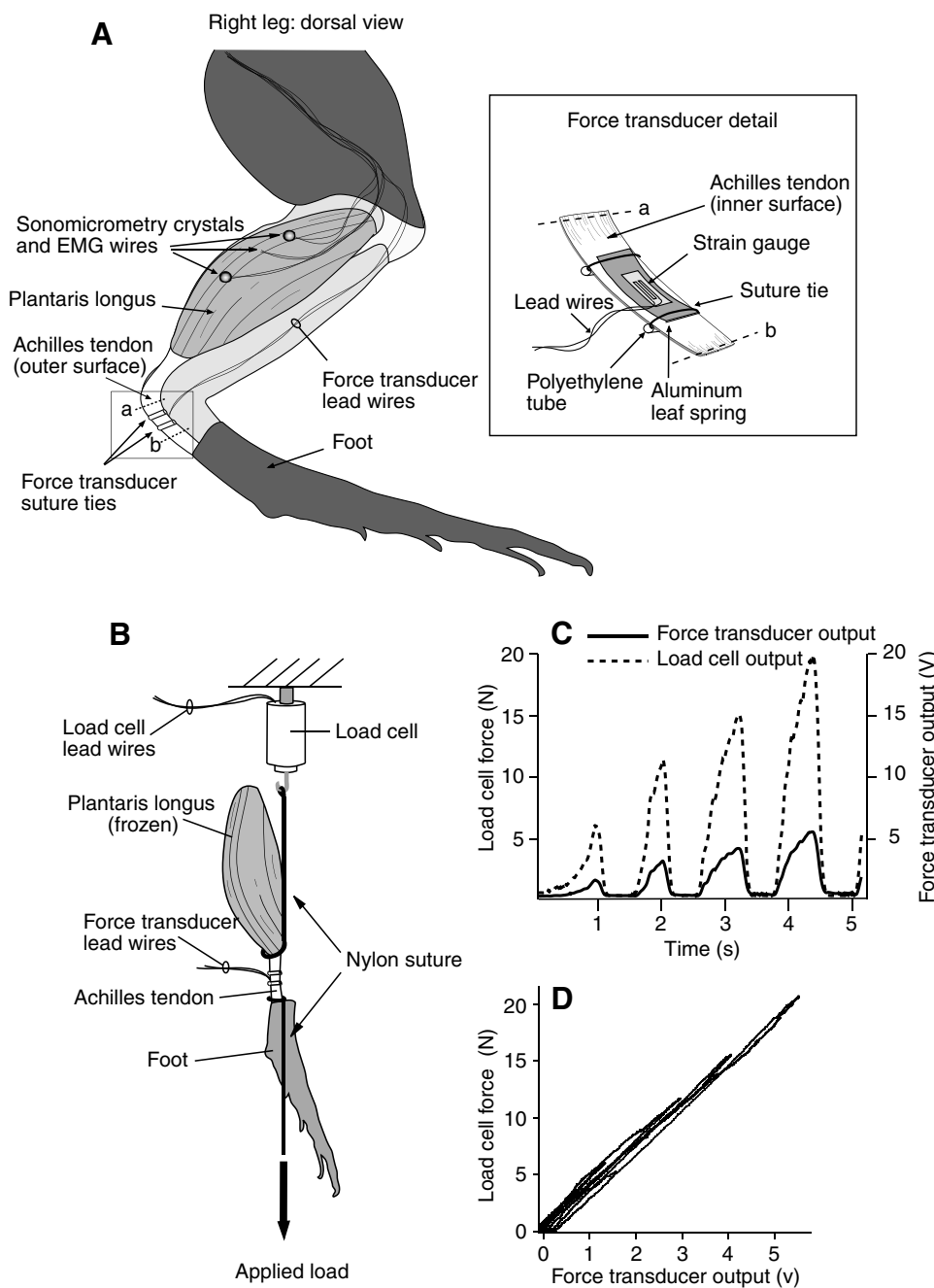


Fig. 1. Electrode implantation and force transducer calibration. (A) Anatomy of the plantaris longus in the *X. laevis* hindlimb showing implantation of electrodes. Muscle activity and changes in muscle fascicle length were measured by bi-polar EMG electrodes and sonomicrometry crystals, respectively. Plantaris longus force was measured by a strain gauge force transducer (inset) tied to the inner surface of the Achilles tendon (see text for further details). (B) Representative tendon force transducer calibration (frog 5). The foot was removed from the animal and the plantaris muscle was mechanically isolated from proximal tissues (see text) allowing the muscle–tendon unit to be mounted in-line with a calibrated load cell in a simple jig. (C) The data record shows force from the calibrated load cell (broken line) and the voltage output from the force transducer (solid line) for a series of loading cycles. (D) Load cell force is plotted against force transducer output to show the linear response of the force transducer over the cycles shown in C.

sutured to the skin over the center of the body. Video sequences were analyzed *via* a custom Labview digitizing program (National Instruments, Austin, TX, USA) to calculate swimming velocities and accelerations.

Measurement of in vivo plantaris force

A novel tendon buckle force transducer was mounted to the Achilles tendon to measure plantaris muscle force *in vivo* (Fig. 1A). The transducer was constructed from a FLK-1-11 1.0 mm strain gauge (TML Co., Ltd, Tokyo, Japan) that was bonded, using an oven cure epoxy (AE-10, Measurements Group, Inc., Raleigh, NC, USA), to the concave surface of a double-layered aluminum leaf spring [layers were cut from the wall of a 12-oz. soda (fizzy drink) can and glued together with a cyanoacrylate adhesive]. The shallow curvature of the aluminum functioned as a leaf spring to allow tensile forces transmitted *via* the muscle's tendon to be measured by the strain gauge as the leaf spring was deflected under the applied load. To allow firm attachment to the tendon during surgery 4.0 silk suture ties were mounted to the ends of the leaf spring with epoxy. Two coats of biologically inert M-coat A polyurethane curing agent (Measurements Group, Inc.) were applied to the leaf spring and lead wire attachments to provide electrical insulation and to minimize tissue irritation.

Force transducer calibration

Following data collection, animals were euthanized by immersion in 0.3% MS-222 for 1 h and the plantaris muscle was cut from its origin at the distal femur (with its insertion at the Achilles tendon left intact). The femur and proximal portions of the tibia and fibula were carefully cut away while keeping the ankle joint and the foot intact. A suture was then tied firmly around the distal end of the plantaris aponeurosis and its junction with the Achilles tendon (at the point of the muscle-tendon junction). The belly of the plantaris was frozen with liquid N₂ to immobilize the suture tie to the tendon. The suture was then secured to a calibrated Kistler load cell (type 9203, Kistler Instrument Corporation, Amherst, NY, USA; Fig. 1B). Pulling directly on the foot, allowed us to calibrate the buckle transducer voltage output to a known tensile force (Fig. 1C,D). Muscle cross sectional area was calculated by the following formula: (muscle mass/muscle length)/muscle density. For comparison across individuals, muscle force was converted to muscle stress by dividing by the muscle cross sectional area. To verify that the buckle did not permanently deform under *in vivo* loading, calibration trials were repeated to show that the tendon leaf spring transducer did not lose sensitivity through repeated loading cycles.

Sonomicrometry

Sonomicrometry crystals provided direct measurement of muscle fascicle length changes. Instantaneous recordings of inter-crystal displacements were obtained by a Triton 120.2 sonomicrometry system (Triton Technology Inc., San Diego, USA). Accurate temporal records of instantaneous fascicle length were obtained after correcting for the speed of sound in skeletal muscle, 1540 m s⁻¹ (Goldman and Hueter, 1956), for the faster speed of sound propagation through the spherical epoxy lens of the crystal [representing a + 0.6 mm correction

(Gillis and Biewener, 2001)], and adjusting for the 5 ms phase delay introduced by the Triton sonomicrometry filters. No correction for fiber pennation angle was required because the plantaris muscle fibers in the region examined within the muscle run parallel to the muscle's force transmission axis.

For measurements of muscle work and power, muscle fascicle strain (ϵ) was first calculated from recordings of muscle fascicle length change (Δl): $\epsilon = \Delta l / l_{\text{rest}}$, where l_{rest} was the fascicle length recorded while the animal was at rest, prior to any swimming activity (with the leg joints in a moderately flexed position). Since the crystals were placed along a fascicle spanning the entire length of the muscle, whole-muscle length changes (ΔL) were then obtained using $\Delta L = \epsilon \times L_{\text{rest}}$, where L_{rest} is the resting length of the entire length of the fascicle. Muscle shortening below L_{rest} was defined as positive strain, whereas muscle lengthening above L_{rest} was defined as negative strain. This approach assumes that all activated fascicles within the muscle contract with similar strain patterns.

Data analysis

Each experimental swimming trial produced a series of propulsive strokes. To calculate work and power for a single swimming stroke cycle, *in vivo* plantaris force and EMG data were partitioned with respect to the muscle strain cycle (a swimming stroke was defined as the period between the onset of muscle shortening and the end of muscle re-lengthening; Fig. 3A, stages 1 and 5, respectively). Work averaged over the entire stroke cycle (cycle work) was calculated by the work loop technique and cycle power was obtained by dividing cycle work by cycle duration (Josephson, 1985). The onset of muscle force was chosen as the point at which force reaches 1% peak force above resting force.

The magnitude of muscle recruitment (EMG intensity) was measured by rectifying the EMG signal and quantifying the average spike amplitude of each burst of activity. EMG phase was calculated as $100 \times (\text{EMG onset time} - \text{shortening onset time}) / \text{stroke duration}$, and EMG duty cycle as $100 \times (\text{duration of EMG activity} / \text{stroke duration})$.

Statistical analysis: multiple regression and path analysis

Data from each individual were treated separately for statistical analysis. For each individual, measurements from all propulsive swimming strokes were treated as independent events. For each swimming stroke, several parameters of muscle performance were measured (Table 2). Multiple least-squares regression (MLSR) was used to partition the relative contributions of these parameters on the variance in *in vivo* plantaris muscle power for each of the six individuals. To correct for variation due to random error in dependent and independent variables, Reduced Major Axis (RMA) regression was used where appropriate (McArdle, 1988; Quinn and Keough, 2002).

Path Analysis was used to assemble separate MLSR tests into an overall statistical model explaining proposed causal relationships between independent variables and response variables. Since each of the individuals was treated separately, we repeated each set of MLSR tests six times (once for each frog). Each independent variable was evaluated by (1) path coefficients (standardized partial regression slopes), which

Table 2. Muscle activation and contractile performance

Performance parameter	Minimum	Maximum	CV averaged across individuals
Power (W kg ⁻¹ muscle)	2.32±2.51	74.17±66.39	0.88±0.28
Work (J kg ⁻¹ muscle)	0.88±0.61	21.50±17.69	0.72±0.18
Cycle duration (s)	0.23±0.07	0.76±0.22	0.31±0.10
Peak stress (kPa)	33.0±16.6	189.9±113.8	0.44±0.06
Strain amplitude (% L_{rest})	9.09±4.44	19.44±8.70	0.23±0.11
EMG phase (% stroke duration)	-18.02±3.24	14.66±10.12	0.36±0.08
EMG duty cycle (% stroke duration)	13.28±2.83	54.12±11.92	0.36±0.07
EMG intensity (V)	0.06±0.04	0.71±0.76	0.67±0.32

CV, coefficient of variation. Values are means ± s.d. (for N values, see text).

Results

Xenopus laevis swimming behavior

During experimental swimming bouts, *X. laevis* hindlimbs generated propulsion underwater by rapidly and synchronously extending the hip, knee, ankle and metatarsal-phalangeal joints of both legs. Experimental bouts of swimming consisted of several propulsive strokes (3–6) followed by a long (up to 5 min) period of rest (Fig. 2). Peak swimming speeds ranged from 0.3±0.1 to 1.1±0.3 m s⁻¹ and peak accelerations ranged from 2.0±1.4 to 18.8±5.0 m s⁻² (mean ± s.d.; $N=3$ frogs).

In vivo plantaris fascicle strain patterns

Individual animals displayed similar basic fascicle strain patterns of their plantaris longus, which could be grouped into propulsive and recovery phases (Fig. 3A,B). Propulsive phases were shorter than the recovery phases and began when the muscle shortened to extend the ankle joint. Following peak shortening (peak ankle extension), the recovery phase began when the muscle passively re-lengthened and the ankle joint flexed to prepare for the following stroke. Although some fascicle strain trajectories were approximately sinusoidal (Fig. 3A), the relative duration of the propulsive phase, on average, was short (36±14% of total cycle duration, mean ± s.d., $N=160$, pooled across six animals).

Within this basic strain regime, plantaris strain patterns exhibited variation both among individuals and among trials of a single individual (compare Fig. 3A with Fig. 4A). Generally, muscle length oscillated asymmetrically about resting muscle length (L_{rest}). However, within individual animals and between trials the magnitude of strain to which the plantaris was stretched above L_{rest} (at the point of peak ankle flexion between propulsive strokes) was consistently uniform, although the magnitude of this stretch varied among individuals. Therefore, stroke-to-stroke changes in total strain amplitude resulted almost entirely from variation in the amount of plantaris shortening (fascicle strain below L_{rest}). Strain amplitude $[(L_{max}-L_{min})/L_{rest}]$ varied not only among trials of an individual animal, but also from stroke to stroke within a trial (Fig. 3A, Fig. 4A). Among individuals, the strain amplitude of the plantaris ranged from 9.09±4.44% to 19.44±8.70% (Table 2; mean ± s.d.).

In vivo plantaris force patterns

During the propulsive phase of each stroke, force increased rapidly at the onset of muscle shortening (Fig. 3B, stage 1),

indicate the strength of the relationship between each independent variable and the dependent variable, and (2) partial determinants of correlation (r^2), which resolve the relative contributions of each independent variable to the total amount of variance observed in the dependent variable (Li, 1975; Wootten, 1994). For independent variables x_1 and x_2 , path coefficients were calculated by the following:

$$\beta_1 = b_1(\sigma_1/\sigma_y); \quad \beta_2 = b_2(\sigma_2/\sigma_y), \quad (1)$$

where β_1 is the path coefficient describing the strength of the relationship between x_1 and y , b_1 is the partial slope of x_1 estimated from MLSR, and σ is the standard deviation (similar definitions apply for β_2 and b_2 relating x_2 to y).

Partial correlation coefficients are then computed from the path coefficients:

$$r_1 = \beta_1 + \beta_2 \times r_{12}, \quad (2)$$

where r_1 is the partial correlation coefficient between x_1 and y , and r_{12} is the simple correlation coefficient between x_1 and x_2 . Eqn 2 is generalized to calculate partial correlation coefficients for multiple independent variables:

$$[r_1 \ r_2 \dots r_j] = [\beta_1 \ \beta_2 \dots \beta_j] \begin{bmatrix} r_{11} & r_{12} \dots r_{1j} \\ r_{21} & r_{22} \dots r_{2j} \\ r_{j1} & r_{j2} \dots r_{jj} \end{bmatrix}, \quad (3)$$

where the vector containing path coefficients for j independent variables is multiplied by the correlation matrix containing correlations between all independent variables. Path coefficients are then multiplied by partial correlation coefficients to partition the components of the coefficient of determination (R^2):

$$R^2 = \beta_1 r_1 + \beta_2 r_2 = r_{x_1}^2 + r_{x_2}^2, \quad (4)$$

where R^2 is the fraction of variance in y explained by all of the independent variables and $\beta_1 r_1$ and $\beta_2 r_2$ describe the partial variance explained by x_1 and x_2 , respectively (Eqn 1, Eqn 2 and Eqn 4) (Li, 1975). We will refer to $\beta_1 r_1$ or $\beta_2 r_2$ as a partial coefficient of determination (r^2), which is not equivalent to r_1^2 (the square of the partial correlation coefficient). Simple least-squares regression statistics were performed using SPSS 13.0 (SPSS Inc., Chicago, IL, USA) and a custom Labview program (National Instruments) was used to compute partial regression and correlation coefficients for path analysis and RMA for multiple regression tests.

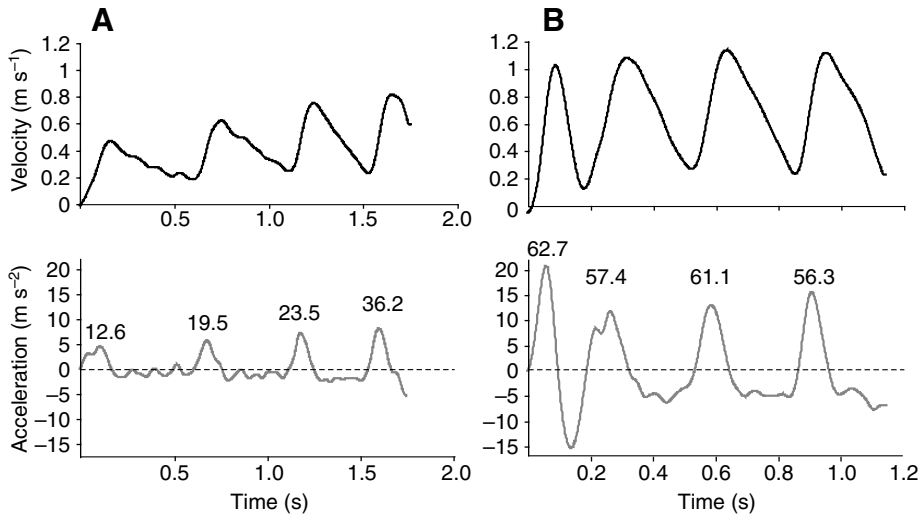


Fig. 2. Representative patterns of swimming velocity and acceleration for frog 6. (A) Moderate speed swimming. Velocities (top) and accelerations (bottom) for four consecutive stroke cycles showing increasing velocity and acceleration digitized from the video sequence of a single trial. (B) Vigorous swimming. Velocities (top) and accelerations (bottom) for four stroke cycles from a contrasting trial of the same frog showing a rapid escape stroke followed by three high velocity strokes. Numbers above each acceleration peak represent the plantaris muscle mass-specific power output (W kg^{-1}) for each cycle.

reaching peak force during the period of the greatest muscle shortening velocity (stage 2). In most frogs observed, peak muscle force correlated positively with the muscle's average shortening velocity ($r^2=0.52\pm 0.21$, $P<0.0001$ for frogs 1, 4–6). The muscle then relaxed, reaching minimum force at $81\pm 12\%$ of the cycle ($45\pm 16\%$ after the onset of muscle re-lengthening). During the recovery phase (stages 3–5) force developed passively within the plantaris muscle–tendon unit as

antagonistic muscles flexed the ankle joint (stage 4) before the muscle was activated for the next propulsive stroke (stage 5). Passive forces varied widely from stroke to stroke and across individuals, averaging $15.5\pm 13.2\%$ of peak cycle force and correlated weakly with peak cycle stress ($r^2=0.25$, $P<0.0001$). To compare across individuals of different size, plantaris muscle forces were normalized to each animal's muscle fiber cross-sectional area to obtain values of peak muscle stress (Table 1).

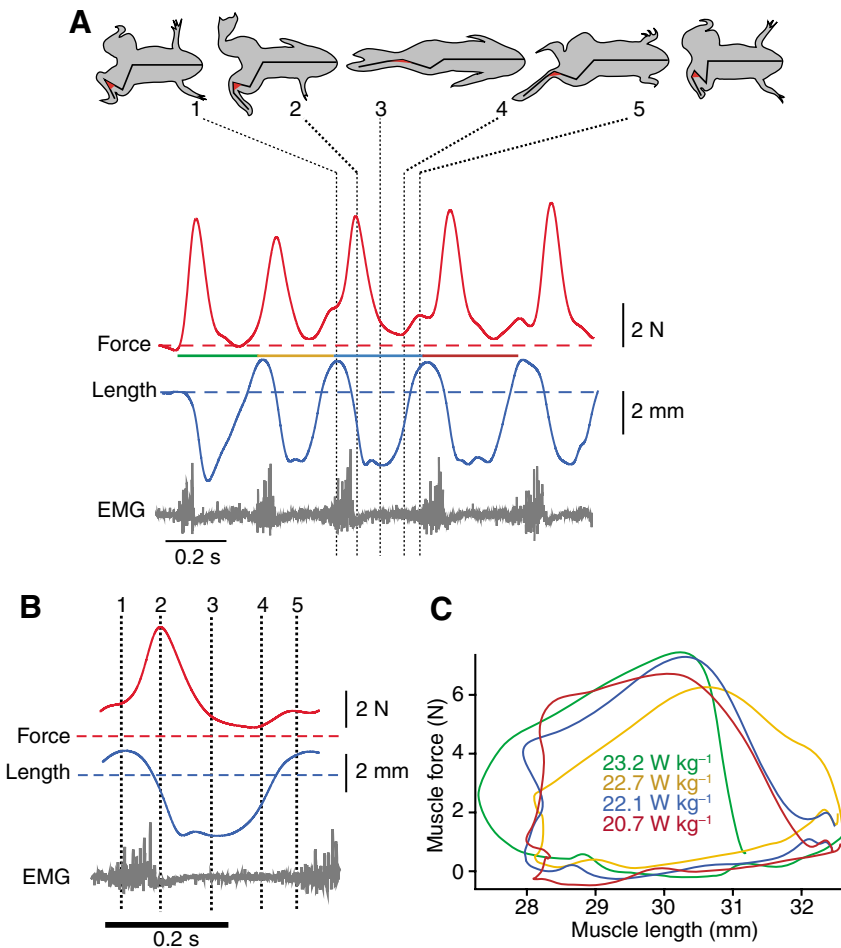


Fig. 3. (A) Representative data recordings of plantaris longus force (red), whole-muscle length (blue), and activation (black) from a single burst swimming trial of frog 5. Broken lines on the length and force traces represent resting muscle length (L_{rest} , measured when the animal was unmoving in the aquarium) and resting force, respectively. Vertical dotted lines (1–5) illustrate kinematic stages defining the stroke cycle. The ankle joint is highlighted in red. A swimming stroke begins with a propulsive phase characterized by rapid joint extension (1–3). The recovery phase that follows (3–5) prepares the limb for the next stroke by returning the leg to its initial configuration. (B) Expanded view of data record to show a single stroke cycle. (C) Four *in vivo* work loops (representing four consecutive swimming strokes) are plotted directly from force–length data shown in the data traces in A. The colored bars above the length trace shown in A match the work loop colors to show how the force–length data were partitioned to calculate work and power. Muscle power (W kg^{-1} muscle) is shown for each stroke.

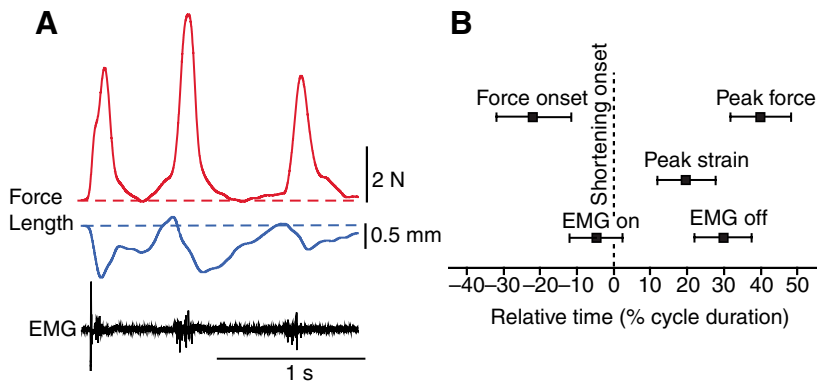


Fig. 4. (A) Data recordings of plantaris longus force (red), whole-muscle length (blue), and activation (black) from frog 4 to show the maximum differences observed between individual animals (compare with Fig. 3A). (B) Diagram showing the variation in the relative timing of force-length activation events among swimming strokes for frog 5. Note that force develops passively at the end of the previous cycle, as the limb is being protracted and the ankle and knee are flexed.

Averaged among all individuals, the maximum *in vivo* stress recorded during experimental swimming trials was 189.9 ± 113.8 kPa (Table 2; $N=6$).

Plantaris neural activation patterns

The timing of plantaris muscle activation was highly variable within and between individual frogs. The muscle was activated 16 ± 40 ms before the onset of fascicle shortening and force development (Fig. 3B, Fig. 4B). Muscle activity continued for 139 ± 61 ms, ceasing 39 ± 63 ms after peak stress and 33 ± 83 ms before peak shortening strain. Consequently, the timing of muscle activation relative to shortening and force development was variable among trials and across individuals. Variation in these timing patterns, however, did not correlate with variation in muscle work or power.

Plantaris work and power output

Nearly all of the force generated by the plantaris during swimming strokes occurred when the muscle was shortening (Fig. 3B, Fig. 4B), resulting in substantial net positive work. This is reflected by the open counterclockwise *in vivo* 'work loops' produced by the plantaris during each contraction cycle (Fig. 3C). Both work and power varied among individuals (Table 2), with frog 1 exhibiting the greatest range (from 1.53 to 55.69 J kg⁻¹ muscle and from 6.94 to 199.21 W kg⁻¹ muscle). Work and power also varied from stroke to stroke within experimental trials. For each of the 53 trials (gathered from all six animals), the range of variation from stroke to stroke within a trial (i.e. the difference between the maximum and minimum work or power recorded within a trial) averaged 7.06 ± 6.56 J kg⁻¹ muscle and 20.36 ± 22.13 W kg⁻¹ muscle for work and power, respectively. For all frogs, there was considerable variation in the timing of force and muscle activation events with respect to strain patterns (Fig. 4B). Consequently, both work loop shape as well as plantaris mass-specific power and work output differed from stroke to stroke (Fig. 3C).

Variation in muscle performance parameters

The large range of variation in swimming performance and plantaris muscle contractile function observed among trials and from stroke to stroke for each frog is summarized in Fig. 5 and Table 2. Muscle mass-specific power, work and EMG intensity showed the highest median coefficient of variation

(CV) within an individual animal (indicating high variability from trial to trial and/or from stroke to stroke) and the broadest interquartile range (indicating high variability across frogs). Median CV for peak muscle stress was high for each individual animal (CV = 0.44 ± 0.06 , mean \pm s.d., $N=6$), but the range of variation was consistent across individuals (interquartile range = 0.04). Conversely, strain amplitude was much less variable within individuals (CV = 0.23 ± 0.13), yet varied substantially among frogs (interquartile range = 0.18). Cycle duration and EMG duty cycle were similarly variable both within individual animals (CV = 0.31 ± 0.1 and 0.36 ± 0.07 , respectively) and between frogs (interquartile range = 0.13 and 0.18, respectively). EMG phase also showed variability both within and among frogs (CV = 0.36 ± 0.08 ; interquartile range = 0.13).

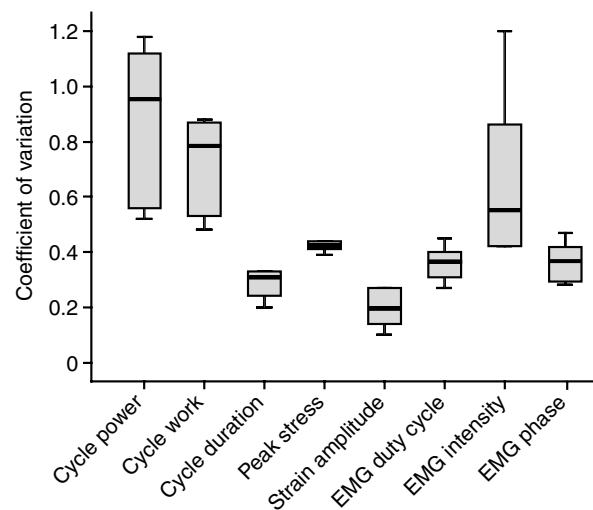


Fig. 5. Box-and-whisker diagram showing the variability of muscle performance parameters within and among individual frogs. For each performance parameter, the coefficient of variation (CV) was found from the data for each frog. The boxes represent 50% of the data range and the whiskers bracket the interquartile range of observed data compared across individuals. Bold horizontal bars represent the median CV found among frogs. High median CV values indicate large variability within individual frogs, whereas broad boxes signify high variability among individuals.

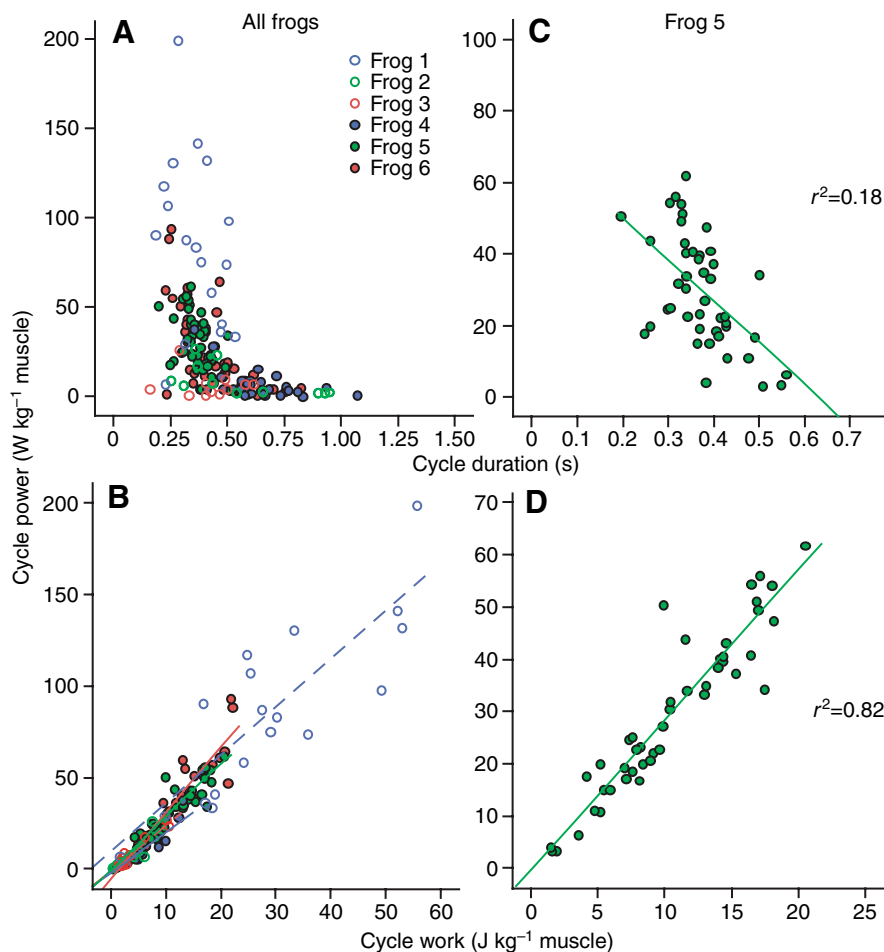


Fig. 6. (A,B) Scatter plots showing the variation in plantaris power output as a function of cycle duration (A) and work (B) for all six individuals. (C,D) Plots for power vs cycle duration (C) and power (D) vs cycle work for frog 5, to exemplify trends seen within individuals. Regression lines for each individual frog were plotted using simple least-squares regression to illustrate general trends in the data. Regression lines that are not statistically significant (tested separately by multiple least-squares regression) are not shown. Solid and broken regression lines (where shown) correspond to data represented by solid circles and open circles, respectively. Partial coefficients of determination (r^2) were calculated from partial least-squares regression and path analysis to account for variance explained by interaction between independent variables (see text). For clarity, regression lines are omitted from A.

Muscle power and muscle impulse versus swimming performance

For the three individuals from which swimming performance was measured, plantaris cycle power output correlated positively with peak swimming speed ($r^2=0.21, 0.60$ and 0.35 , $P<0.01$) and peak acceleration ($r^2=0.44, 0.36$ and 0.28 , $P<0.0001$ for frogs 4, 5 and 6, respectively). Additionally, we found that muscle impulse (the time integral of muscle force) also correlates positively with peak acceleration ($r^2=0.29, 0.22, 0.60$, $P<0.01$ for frogs 4, 5 and 6, respectively).

Muscle power versus work and cycle duration

Multiple least-squares regression revealed that plantaris mass-specific power output was most significantly correlated with cycle work and cycle duration ($P<0.05$, Fig. 6). As expected, cycle work correlated positively with cycle power, whereas cycle duration correlated negatively ($\beta=0.93\pm 0.06$ and -0.30 ± 0.15 , respectively; Fig. 7A, Table 3). Partial least-squares regression tests on data from individual frogs indicate that variation in cycle work and cycle duration accounted for $88\pm 5\%$ and $12\pm 5\%$ ($N=6$) of the variation in power, respectively (Table 3).

Muscle work versus fascicle strain amplitude and stress

In five out of six frogs, muscle work correlated positively with peak muscle stress ($\beta=0.87\pm 0.14$, $P<0.05$, for frogs 2–5).

In two out of six animals, work also correlated positively, but less strongly, with fascicle strain amplitude ($\beta=0.21\pm 0.12$, $P<0.05$; Fig. 7A, Fig. 8, Table 3). Peak stress contributed significantly to the multiple linear regression model, predicting $80\pm 12\%$ of the variation in muscle work (frogs 2–6, Table 3). However, fascicle strain amplitude contributed significantly in only two animals, explaining $17\pm 14\%$ of the variance in muscle work (frogs 4 and 5, Fig. 7A, Table 3). EMG phase and EMG duty cycle did not contribute significantly to variation in cycle work ($P>0.05$).

Peak muscle stress versus EMG intensity and EMG duty cycle

Peak muscle stress correlated with EMG intensity, but less strongly with EMG duty cycle ($\beta=0.76\pm 0.16$ and 0.29 ± 0.14 , respectively; Fig. 7A, Fig. 9, Table 3). EMG intensity was the strongest covariate in the multiple linear regression model, accounting for $53\pm 20\%$ (frogs 1, 2, 3–6) of the variation in peak stress. EMG duty cycle explained only $11\pm 9\%$ (frogs 3–6) of the variance in peak muscle stress (Fig. 7A), and EMG phase failed to contribute significantly to the regression model ($P>0.05$).

Discussion

Modulation of plantaris muscle power during burst swimming

The goal of our study was to investigate how underlying components of *X. laevis* plantaris muscle performance (muscle

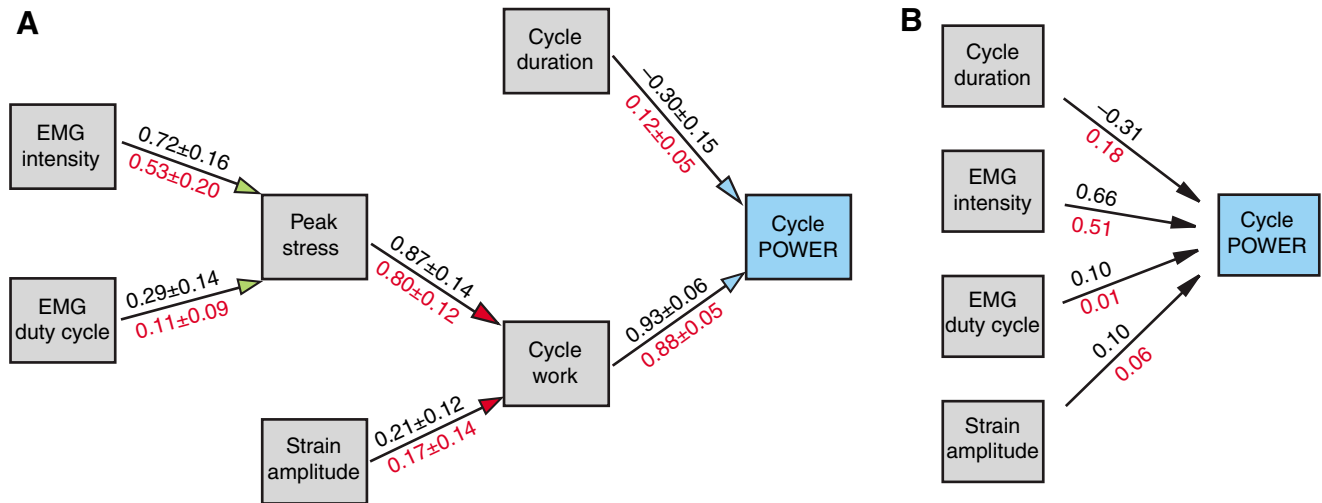


Fig. 7. A statistical model explaining the relationships of all measured muscle performance parameters in relation to muscle power output. (A) Path diagram summarizing the results from three separate multiple regression tests. Arrows pointing from each independent variable to a dependent variable represent relationships revealed by one multiple regression test. Colored arrowheads identify the three separate tests. Test 1: cycle power vs cycle work and cycle duration (blue); Test 2: cycle work vs peak stress and strain amplitude (red); Test 3: peak stress vs EMG intensity and EMG duty cycle (green). Black numbers above the arrows are path coefficients and red numbers below the arrows are partial coefficients of determination ($r^2 = \text{path coefficient} \times \text{partial correlation coefficient}$) describing the fractional variance explained by each covariate. Values are mean \pm s.d. for all frogs that demonstrated a significant correlation ($P \leq 0.05$). (B) Reduced path diagram summarizing data from a single frog (frog 5) indicates that four primary performance parameters (cycle duration, EMG intensity, EMG duty cycle and strain amplitude) explain approximately 76% of the variance in plantaris power. Black numbers represent path coefficients and red numbers partial coefficients of determination; these are given for each individual frog in Table 3. Independent variables that did not significantly contribute to the regression model ($P > 0.05$) are not included in the average values shown on the path diagrams.

stress, strain, strain rate and neural activation) varied to modulate muscle power output over a wide range of natural swimming performance. As expected, muscle power correlated significantly with swimming speed and acceleration, suggesting that these parameters of muscle performance are good predictors of the hydrodynamic requirements of swimming. Among these parameters, peak muscle stress was the strongest predictor of variation in plantaris muscle cycle work and power across the range of swimming strokes recorded. Based on an earlier study that examined the modulation of muscle power output during flight in cockatiels (Hedrick et al., 2003), we predicted that cycle work would be a strong correlate to muscle power in swimming frogs. Additionally, we expected an equally strong, but negative correlation between cycle duration (1/cycle frequency) and muscle power output. This prediction follows from observations of fish in which increased swimming speed is enabled by increases in EMG burst frequency and intensity of myotomal red muscle activity (Freadman, 1979), reinforced by additional recruitment of white muscle fibers at faster speeds (Rome et al., 1984). *In vitro* work loop studies (Altringham and Johnston, 1990a; Coughlin et al., 1996b; Altringham and Block, 1997; Syme and Shadwick, 2002) also show that, over a particular range of frequencies, power increases with cycle frequency. Our data are consistent with these findings for fish myotomal muscle and swimming performance, supporting the hypothesis that cycle duration inversely correlates with muscle power output. However, the influence of cycle work on power output was much greater than expected, contributing to $88 \pm 5\%$ of the variation in power, with the remaining $12 \pm 5\%$ predicted by cycle duration. The dominance of work performance over cycle duration for

determining muscle power reflects differences in stroke-to-stroke variation between these two parameters (CV = 0.72 ± 0.18 for cycle work vs 0.31 ± 0.10 for cycle duration, Table 2, Fig. 5).

Underlying components of plantaris work modulation

Because muscle power output is determined by net work divided by cycle duration, other parameters indirectly contributed to variation in power output by modulating plantaris work. For five out of six frogs, peak cycle stress explained $80 \pm 12\%$ of the variation in cycle work, and therefore accounted for $71 \pm 11\%$ of the variance in power. In addition to peak stress, past studies have demonstrated that strain amplitude is an important determinant of muscle work and power output under both *in vitro* (e.g. Josephson, 1985; Full et al., 1998) and *in vivo* (Daley and Biewener, 2003; Hedrick et al., 2003) conditions. Therefore, we expected a similar finding in swimming frogs. Contrary to our expectations, differences in strain amplitude had a significant effect on cycle work in only two individuals (frogs 4 and 5, $P = 0.0104$ and 0.0354 , respectively), accounting for $17 \pm 14\%$ of the variation in cycle work (and $15 \pm 13\%$ of the variance in power; Table 3). For the other four animals, the remaining 10–20% of variance in work was neither explained by peak cycle stress nor strain amplitude.

This unexplained variation in cycle work suggests that simple measures of instantaneous peak force and peak strain amplitude may not fully predict the work and power requirements of a muscle. Additional parameters, such as muscle impulse [the time integral of muscle force (Altringham and Johnston, 1990b)], the rate of force development and force relaxation (Askew and Marsh, 1998), and the relative timing of force

Table 3. Path analysis results from three separate multiple regression tests for individual frogs (see Fig. 7)

Test 1: Power vs duration and work						
Frog	Power vs duration			Power vs work		
	β	r^2	P	β	r^2	P
1	-0.52	0.16	<0.0001*	0.97	0.85	<0.0001*
2	-0.25	0.15	<0.0001*	0.87	0.85	<0.0001*
3	-0.43	0.08	<0.0001*	1.02	0.94	<0.0001*
4	-0.17	0.09	<0.0001*	0.92	0.91	<0.0001*
5	-0.31	0.18	<0.0001*	0.86	0.82	<0.0001*
6	-0.12	0.08	0.001*	0.92	0.92	<0.0001*
Mean**	-0.30	0.12	–	0.93	0.88	–
s.d.	0.15	0.05	–	0.06	0.05	–

Test 2: Work vs strain and stress						
Frog	Work vs strain			Work vs stress		
	β	r^2	P	β	r^2	P
1	0.37	0.28	0.3266	0.42	0.31	0.2575
2	0.22	0.12	0.5491	1.03	0.89	0.0021*
3	0.13	0.10	0.7462	0.79	0.71	0.0052*
4	0.29	0.27	0.0104*	0.68	0.65	<0.0001*
5	0.12	0.07	0.0354*	0.86	0.80	<0.0001*
6	-0.04	0.02	0.5596	0.99	0.95	<0.0001*
Mean**	0.21	0.17	–	0.87	0.80	–
s.d.	0.12	0.14	–	0.14	0.12	–

Test 3: Stress vs duty cycle and EMG intensity						
Frog	Stress vs duty cycle			Stress vs EMG intensity		
	β	r^2	P	β	r^2	P
1	0.24	0.02	0.2727	0.79	0.54	0.0002*
2	0.02	0.00	0.9958	0.73	0.53	0.0096*
3	0.33	0.11	0.3935	0.28	0.08	0.4861
4	0.38	0.17	<0.0001*	0.73	0.56	<0.0001*
5	0.13	0.01	0.0434*	0.89	0.78	<0.0001*
6	0.36	0.15	0.0006*	0.45	0.22	<0.0001*
Mean**	0.29	0.11	–	0.72	0.53	–
s.d.	0.14	0.09	–	0.16	0.20	–

*Significant ($P < 0.05$); **mean values were averaged over all statistically significant coefficient values.

development and muscle shortening (Josephson and Stokes, 1989; Askew and Marsh, 1997; Daley and Biewener, 2003; Gabaldon et al., 2004) can also be important determinants of work performance. More broadly, across various species and muscles, differences in muscle strain and shortening velocity strongly affect muscle power output. For example, the wallaby plantaris muscle produces minimal work during steady speed hopping by generating force under nearly isometric conditions (Biewener et al., 1998), whereas the quail pectoralis muscle produces near maximal cycle work and power during take-off by maintaining high shortening velocities during force production (Askew and Marsh, 2001). The plantaris muscle in *X. laevis* operates between these two functional extremes, producing positive work by generating force during shortening. However, its work and power output are sub-maximal because

the magnitude of muscle recruitment varies from stroke to stroke (see below).

Timing of muscle shortening velocity and force

Despite the considerable stroke-to-stroke variation observed in cycle work and power output across all frogs, peak muscle stress and peak shortening velocity occurred nearly simultaneously, within the same 10% of cycle duration. This finding is consistent with observations that the plantaris muscle in swimming frogs remains active throughout a significant portion of the muscle shortening period (Kamel et al., 1996; Gillis and Biewener, 2000), suggesting that force develops during rapid shortening to generate work for propulsion. This tight coupling of the timing of shortening velocity and stress may reflect the dependence of muscle stress and strain patterns on the time-varying hydrodynamic drag force exerted on the frog's foot. Because drag is proportional to the square of foot velocity relative to the surrounding fluid (Vogel, 1994) and the plantaris muscle generates force to oppose this drag, peak muscle stress is likely to correlate strongly with foot velocity. Given this, we expected peak muscle stress to occur at maximum ankle extension velocity (and hence, maximum plantaris shortening velocity). This was supported by our observation that peak ankle extension velocity, peak plantaris stress and peak shortening velocity all occurred at similar times in the stroke cycle ($12.9 \pm 18.9\%$, $19.7 \pm 7.9\%$ and $24 \pm 15.4\%$, mean \pm s.d., respectively; Fig. 10). Consequently, peak stress always occurred when the muscle shortened at near peak strain rate, so that the muscle's average strain rate was significantly correlated with force in most frogs observed (see Results).

Relationship between EMG intensity and force

In five out of six animals, EMG burst intensity correlated positively with peak cycle stress ($r^2 = 0.53 \pm 0.20$, Fig. 7A, Fig. 9, Table 3), consistent with the modulation of motor unit recruitment as the mechanical demands on the muscle change from stroke to stroke. This has been observed in other studies of *in vivo* muscle work across a range of locomotor performance (e.g. Daley and Biewener, 2003; Hedrick et al., 2003). However, EMG intensity and stress are not always well correlated. In the turkey lateral gastrocnemius, Roberts et al. (Roberts et al., 1997) observed that EMG intensity and fascicle strain increased during incline running, but muscle stress remained constant. In swimming frogs, the correlation between EMG intensity and muscle stress may be stronger than in running turkeys because increased muscle recruitment likely results in more rapid ankle extension (and therefore greater foot velocity and hydrodynamic force). In order to increase power output from one stroke to the next, the plantaris may also generate the same magnitude of force in a shorter duration. However, this requires the nervous system to recruit additional muscle fibers to compensate for each fiber's diminishing ability to produce force as its shortening velocity increases (Hill, 1938).

Although EMG intensity is a strong predictor of peak muscle stress, instantaneous muscle force depends on several interacting parameters, which our multiple linear regression analysis does not address. These parameters include force-length and force-velocity effects, as well as length and velocity-dependent activation and deactivation effects (Askew

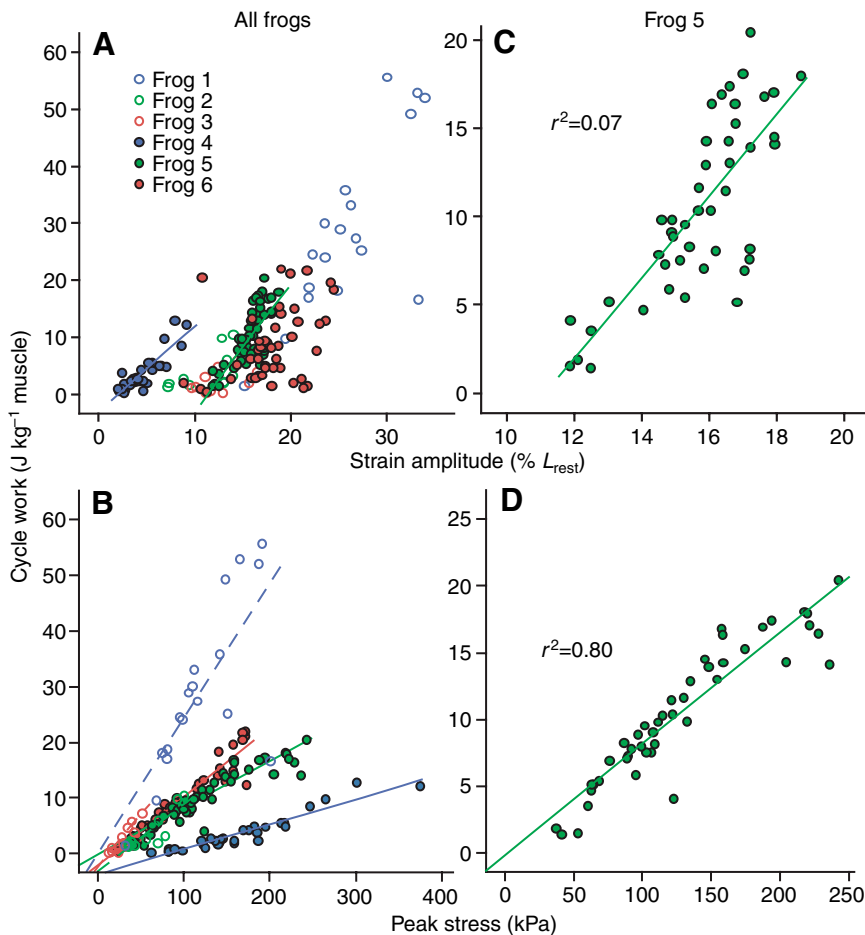


Fig. 8. (A,B) Scatter plots showing the variation in plantaris cycle work as a function of strain amplitude (A) and peak stress (B) for all six individuals. (C,D) Plots for work vs strain amplitude (C) and work vs peak stress (D) for frog 5. Regression lines and partial coefficients of determination (r^2) were calculated in the same manner as in Fig. 6.

and Marsh, 1998; Josephson, 1999). Additionally, muscle force depends on the time-varying external load (Josephson, 1999; Marsh, 1999). For example, Hedrick et al. (Hedrick et al., 2003) suggested that differences in stroke-to-stroke wing position may influence aerodynamic resistance on the wing, introducing a source of variation in muscle force, in addition to that due to changes in muscle recruitment. Similarly, swimming frogs may alter either foot shape or orientation with respect to flow, and thereby affect muscle force by varying where the muscle operates on its force–velocity curve.

Timing of muscle EMG and force development

Because the time course of muscle force with respect to shortening can affect work output, we expected the onset of EMG activity relative to the onset of shortening (EMG phase) to significantly affect cycle work. Surprisingly, however, we found no significant correlation between these two parameters ($P>0.05$). Moreover, EMG phase failed to correlate with any of the muscle parameters examined, despite the observed variation in EMG phase from stroke to stroke (Fig. 5). This result is unexpected, given that many *in vitro* work-loop studies have shown that cyclical work is highly sensitive to EMG phase (Luiker and Stevens, 1993; Rome et al., 1993; Marsh and Olson, 1994; Tu and Dickinson, 1994; Full et al., 1998; Ahn et al., 2003), as this determines whether a muscle develops force during shortening (generating energy) or during lengthening (absorbing energy). Our finding does not exclude the possibility

that EMG phase modulation may influence work and power output *in vivo* in swimming frogs. However, there was no evidence for this given the change in other components of muscle power over the range of swimming performance that we observed. For three out of six frogs, the duration of EMG activity relative to cycle duration (EMG duty cycle) showed a positive, but weak, relationship to peak cycle stress (Table 3), suggesting that higher stresses required longer bursts of activity relative to the cycle duration. Despite this trend, a clearer understanding of how patterns of muscle recruitment and strain affect muscle work and power output will benefit from *in vitro* studies of cyclical muscle work performance that allow controlled muscle strain and activation conditions.

Muscle power and anuran swimming performance

Anurans have served as a model to characterize *in vivo* muscle function during swimming (Kamel et al., 1996; Gillis and Biewener, 2000; Gillis, 2007) as well as to explore how hydrodynamics influence swimming performance (Gal and Blake, 1988; Nauwelaerts et al., 2001; Nauwelaerts and Aerts, 2003; Johansson and Lauder, 2004; Nauwelaerts et al., 2005; Stamhuis and Nauwelaerts, 2005). The present study adds to this current understanding by providing a link between the hydrodynamic requirements of swimming and *in vivo* muscle function. We found that muscle power and muscle impulse both correlate with swimming acceleration. This result corroborates recent studies that have proposed that frogs modulate swimming

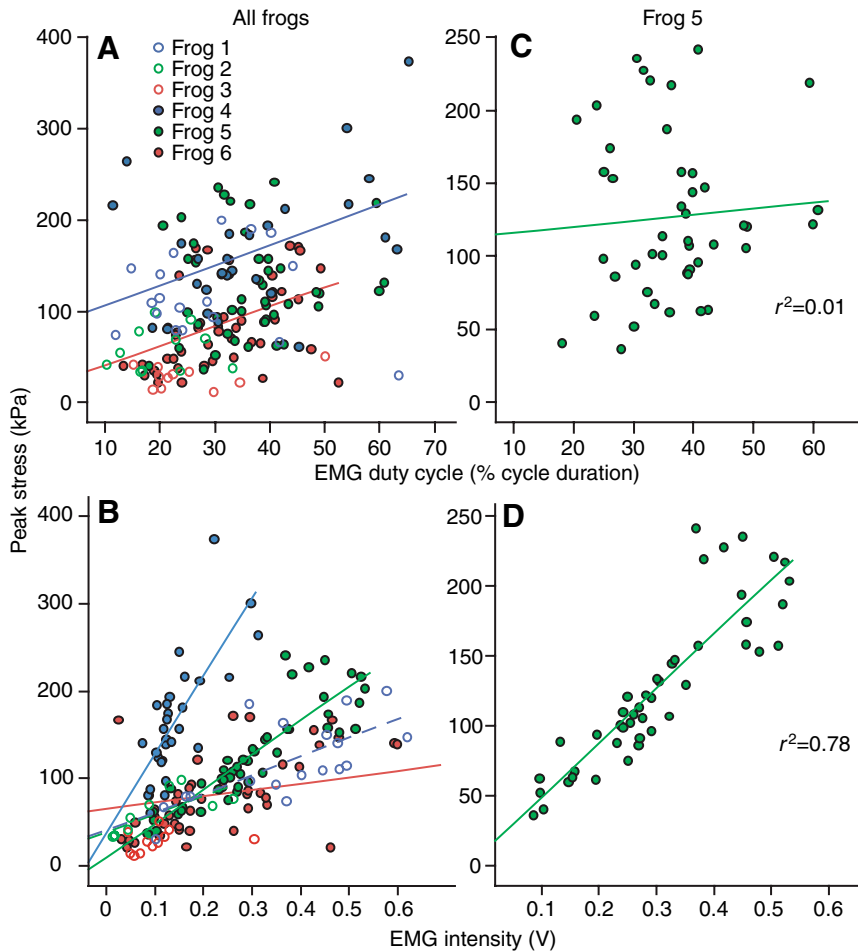


Fig. 9. (A,B) Scatter plots showing variation in peak plantaris stress as a function of EMG duty cycle (A) and EMG intensity (B) for all six individuals. (C,D) Plots for peak stress vs EMG duty cycle (C) and peak stress vs EMG intensity (D) for frog 5. Regression lines and partial coefficients of determination (r^2) were calculated in the same manner as in Fig. 6.

performance by varying the propulsive impulse generated by the feet to overcome drag and added mass forces on the body (Nauwelaerts et al., 2001; Nauwelaerts and Aerts, 2003).

Power requirements of swimming

The variability of plantaris power output observed in *X. laevis* swimming bouts suggests that the hydrodynamic power requirements of anuran swimming can be highly variable from stroke to stroke, particularly when animals swim over a broad range of speeds and accelerations. Our multiple linear

regression and path analysis suggest that this demand to produce variable power output is met principally by changes in plantaris peak muscle stress and, to a lesser extent, changes in the cycle duration (*via* changes in muscle shortening velocity). However, we believe it unlikely that maximum performance of the plantaris in *X. laevis* (and likely other anurans) necessarily limits the animal’s maximum swimming performance. Other muscles (such as proximal extensors of the hindlimb) are likely to contribute significantly to swimming performance. Moreover, even for the most powerful swimming strokes that we observed, the plantaris muscle appeared to generate sub-maximal power. Although our highest observed net power output averaged 200 W kg^{-1} muscle, most frogs produced far less power (74.17 ± 66.39 , Table 2), substantially below the theoretical limit of sustained cycle power for striated skeletal muscle: 250 W kg^{-1} muscle (Weis-Fogh and Alexander, 1977). Rather than limiting the animal’s maximum swimming performance, our results suggest that the plantaris functions to modulate hydrodynamic work, enabling a wide range of swimming performance. We believe this will hold for other muscles used to power swimming in animals, as this is necessary to accommodate the variable hydrodynamic demands for generating propulsion across a range of swimming behaviors.

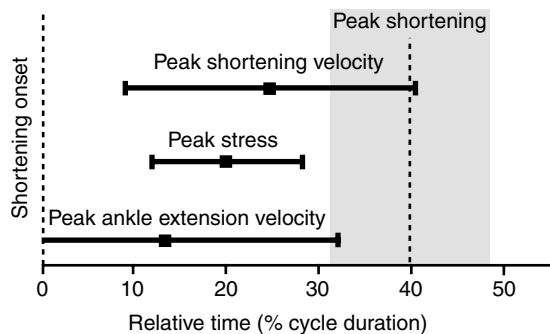


Fig. 10. Diagram showing the relative timing of peak ankle extension velocity, peak plantaris muscle stress, peak muscle shortening velocity and peak muscle shortening. Black squares and whiskers show mean \pm s.d. for frog 5 ($N=45$ swimming strokes).

We thank Pedro Ramirez for animal care and Anna Ahn for invaluable advice with surgical preparation, sonomicrometry and data analysis. We also thank Andrew Carroll, Russell

Main, Em Standen and two anonymous reviewers for helpful comments on earlier drafts of this manuscript.

References

- Ahn, A. N., Monti, R. J. and Biewener, A. A. (2003). *In vivo* and *in vitro* heterogeneity of segment length changes in the semimembranosus muscle of the toad. *J. Physiol.* **549**, 877-888.
- Altringham, J. and Block, B. (1997). Why do tuna maintain elevated slow muscle temperatures? Power output of muscle isolated from endothermic and ectothermic fish. *J. Exp. Biol.* **200**, 2617-2627.
- Altringham, J. D. and Ellerby, D. (1999). Fish swimming: patterns in muscle function. *J. Exp. Biol.* **202**, 3397-3403.
- Altringham, J. D. and Johnston, I. A. (1990a). Modeling muscle power output in a swimming fish. *J. Exp. Biol.* **148**, 395-402.
- Altringham, J. D. and Johnston, I. A. (1990b). Scaling effects on muscle function: power output of isolated fish muscle fibers performing oscillatory work. *J. Exp. Biol.* **151**, 453-467.
- Askew, G. N. and Marsh, R. (1997). The effects of length trajectory on the mechanical power output of mouse skeletal muscles. *J. Exp. Biol.* **200**, 3119-3131.
- Askew, G. N. and Marsh, R. L. (1998). Optimal shortening velocity (V/V_{max}) of skeletal muscle during cyclical contractions: length-force effects and velocity-dependent activation and deactivation. *J. Exp. Biol.* **201**, 1527-1540.
- Askew, G. N. and Marsh, R. L. (2001). The mechanical power output of the pectoralis muscle of blue-breasted quail (*Coturnix chinensis*): the *in vivo* length cycle and its implications for muscle performance. *J. Exp. Biol.* **204**, 3587-3600.
- Biewener, A. A. and Corning, W. R. (2001). Dynamics of mallard (*Anas platyrhynchos*) gastrocnemius function during swimming versus terrestrial locomotion. *J. Exp. Biol.* **204**, 1745-1756.
- Biewener, A., Konieczynski, D. and Baudinette, R. (1998). *In vivo* muscle force-length behavior during steady-speed hopping in tammar wallabies. *J. Exp. Biol.* **201**, 1681-1694.
- Brill, R. W. and Dizon, A. E. (1979). Red and white muscle fibre activity in swimming skipjack tuna, *Katsuwonus pelamis* (L.). *J. Fish Biol.* **15**, 679-685.
- Coughlin, D., Valdes, L. and Rome, L. (1996a). Muscle length changes during swimming in scup: sonomicrometry verifies the anatomical high-speed cine technique. *J. Exp. Biol.* **199**, 459-463.
- Coughlin, D., Zhang, G. and Rome, L. (1996b). Contraction dynamics and power production of pink muscle of the scup (*Stenotomus chrysops*). *J. Exp. Biol.* **199**, 2703-2712.
- Daley, M. A. and Biewener, A. A. (2003). Muscle force-length dynamics during level *versus* incline locomotion: a comparison of *in vivo* performance of two guinea fowl ankle extensors. *J. Exp. Biol.* **206**, 2941-2958.
- Freadman, M. (1979). Role partitioning of swimming musculature of striped Bass, *Morone saxatilis* Walbaum and Bluefish, *Pomatomus saltatrix* L. *J. Fish Biol.* **15**, 417-423.
- Full, R. J., Stokes, D. R., Ahn, A. N. and Josephson, R. K. (1998). Energy absorption during running by leg muscles in a cockroach. *J. Exp. Biol.* **201**, 997-1012.
- Gabaldon, A. M., Nelson, F. E. and Roberts, T. J. (2004). Mechanical function of two ankle extensors in wild turkeys: shifts from energy production to energy absorption during incline *versus* decline running. *J. Exp. Biol.* **207**, 2277-2288.
- Gal, J. M. and Blake, R. W. (1988). Biomechanics of frog swimming. II. Mechanics of the limb-beat cycle in *Hymenochirus Boettgeri*. *J. Exp. Biol.* **138**, 413-429.
- Gillis, G. B. (2007). The role of hind limb flexor muscles during swimming in the toad, *Bufo marinus*. *Zoology* **110**, 28-40.
- Gillis, G. B. and Biewener, A. A. (2000). Hindlimb extensor muscle function during jumping and swimming in the toad (*Bufo marinus*). *J. Exp. Biol.* **203**, 3547-3563.
- Gillis, G. B. and Biewener, A. A. (2001). Hindlimb muscle function in relation to speed and gait: *in vivo* patterns of strain and activation in a hip and knee extensor of the rat (*Rattus norvegicus*). *J. Exp. Biol.* **204**, 2717-2731.
- Goldman, D. E. and Hueter, T. F. (1956). Tabular data of the velocity and absorption of high-frequency sound in mammalian tissues. *J. Acoust. Soc. Am.* **28**, 35-37.
- Hedrick, T. L., Tobalske, B. W. and Biewener, A. A. (2003). How cockatiels (*Nymphicus hollandicus*) modulate pectoralis power output across flight speeds. *J. Exp. Biol.* **206**, 1363-1378.
- Hill, A. V. (1938). The heat of shortening and the dynamic constants of muscle. *Proc. R. Soc. Lond. B Biol. Sci.* **126**, 136-195.
- Hill, A. V. (1970). *First and Last Experiments in Muscle Mechanics*. London: Cambridge University Press.
- Johansson, L. C. and Lauder, G. V. (2004). Hydrodynamics of surface swimming in leopard frogs (*Rana pipiens*). *J. Exp. Biol.* **207**, 3945-3958.
- Josephson, R. K. (1985). The mechanical power output from striated muscle during cyclic contraction. *J. Exp. Biol.* **114**, 493-512.
- Josephson, R. K. (1999). Dissecting muscle power output. *J. Exp. Biol.* **202**, 3369-3375.
- Josephson, R. K. and Stokes, D. R. (1989). Strain, muscle length and work output in a crab muscle. *J. Exp. Biol.* **145**, 45-61.
- Kamel, L. T., Peters, S. E. and Bashor, D. P. (1996). Hopping and swimming in the leopard frog, *Rana pipiens*. II. A comparison of muscle activities. *J. Morphol.* **230**, 17-31.
- Lafferty, K. D. and Page, C. J. (1997). Predation on the endangered tidewater goby, *Eucyclogobius newberryi*, by the introduced African clawed frog, *Xenopus laevis*, with notes on the frog's parasites. *Copeia* **1997**, 589-592.
- Li, C. C. (1975). *Path Analysis: A Primer*. Pacific Grove: The Boxwood Press.
- Luiker, E. A. and Stevens, E. D. (1991). Effect of stimulus frequency and duty cycle on force and work in fish muscle. *Can. J. Zool.* **70**, 1135-1139.
- Luiker, E. A. and Stevens, E. D. (1993). Effect of stimulus train duration and cycle frequency on the capacity to do work in the pectoral fin muscle of the pumpkinseed sunfish, *Lepomis gibbosus*. *Can. J. Zool.* **71**, 2185-2189.
- Marsh, R. L. (1999). How muscles deal with real-world loads: the influence of length trajectory on muscle performance. *J. Exp. Biol.* **202**, 3377-3385.
- Marsh, R. L. and Olson, J. M. (1994). Power output of scallop adductor muscle during contractions replicating the *in vivo* mechanical cycle. *J. Exp. Biol.* **193**, 139-156.
- Marsh, R. L., Olson, J. M. and Guzik, S. K. (1992). Mechanical performance of scallop adductor muscle during swimming. *Nature* **357**, 411-413.
- McArdle, B. H. (1988). The structural relationship: regression in biology. *Can. J. Zool.* **66**, 2329-2339.
- Nauwelaerts, S. and Aerts, P. (2003). Propulsive impulse as a covarying performance measure in the comparison of the kinematics of swimming and jumping in frogs. *J. Exp. Biol.* **206**, 4341-4351.
- Nauwelaerts, S., Aerts, P. and D'Août, K. (2001). Speed modulation in swimming frogs. *J. Mot. Behav.* **33**, 265-272.
- Nauwelaerts, S., Stamhuis, E. J. and Aerts, P. (2005). Propulsive force calculations in swimming frogs. I. A momentum-impulse approach. *J. Exp. Biol.* **208**, 1435-1443.
- Quinn, G. P. and Keough, M. J. (2002). *Experimental Design and Data Analysis for Biologists*. Cambridge: Cambridge University Press.
- Roberts, T. J. and Scales, J. A. (2004). Mechanical power output during running accelerations. *J. Exp. Biol.* **205**, 1485-1494.
- Roberts, T. J., Marsh, R. L., Weyand, P. G. and Taylor, C. R. (1997). Muscular force in running turkeys: the economy of minimizing work. *Science* **275**, 1113-1115.
- Rome, L. C., Loughna, P. T. and Goldspink, G. (1984). Muscle fiber activity in carp as a function of swimming speed and muscle temperature. *Am. J. Physiol.* **247**, R272-R279.
- Rome, L. C., Funke, R. P., Alexander, R. M., Lutz, G., Aldridge, H., Scott, F. and Freadman, M. (1988). Why animals have different muscle fiber types. *Nature* **335**, 824-827.
- Rome, L. C., Swank, D. and Corda, D. (1993). How fish power swimming. *Science* **261**, 340-342.
- Rome, L. C., Swank, D. and Coughlin, D. (2000). The influence of temperature on power production during swimming. II. Mechanics of red muscle fibres *in vivo*. *J. Exp. Biol.* **203**, 333-345.
- Stamhuis, E. J. and Nauwelaerts, S. (2005). Propulsive force calculations in swimming frogs. II. Application of a vortex ring model to DPIV data. *J. Exp. Biol.* **208**, 1445-1451.
- Swank, D. and Rome, L. C. (2000). The influence of temperature on power production during swimming. I. *In vivo* length change and stimulation pattern. *J. Exp. Biol.* **203**, 321-331.
- Syme, D. A. and Shadwick, R. E. (2002). Effects of longitudinal body position and swimming speed on mechanical power of deep red muscle from skipjack tuna (*Katsuwonus pelamis*). *J. Exp. Biol.* **205**, 189-200.
- Tu, M. and Dickinson, M. (1994). Modulation of negative work output from a steering muscle of the blowfly *Calliphora vicina*. *J. Exp. Biol.* **192**, 207-224.
- Vogel, S. (1994). *Life in Moving Fluids*. Princeton: Princeton University Press.
- Weis-Fogh, T. and Alexander, R. M. (1977). The sustained power output from striated muscle. In *Scale Effects in Animal Locomotion* (ed. T. J. Pedley), pp. 511-525. London: Academic Press.
- Wootton, J. T. (1994). Predicting direct and indirect effects: an integrated approach using experiments and path analysis. *Ecology* **75**, 151-165.